INT. J. REMOTE SENSING, 2002, VOL. 23, NO. 15, 2939–2950

An automated cloud detection method for daily NOAA-14 AVHRR data for Texas, USA

P. Y. CHEN*, R. SRINIVASAN

Spatial Sciences Laboratory, Department of Forest Science, Texas A&M University, College Station, Texas 77843, USA

G. FEDOSEJEVS

Canada Center for Remote Sensing, 588 Booth Street, Ottawa, Ontario K1A 0Y7, Canada

and B. NARASIMHAN

Department of Agricultural Engineering, Texas A&M University, College Station, Texas 77843, USA

(*Received 11 July 2000; in final form 22 May 2001*)

Abstract. A variety of cloud types appears in each Advanced Very High Resolution Radiometer (AVHRR) image. Clouds may contaminate solar reflectance data to be used for vegetation studies. This may jeopardize the accuracy of any quantitative results from data analysis. Published cloud detection algorithms for AVHRR data to date have mainly used data over Europe received from the National Oceanic and Atmospheric Administration (NOAA)-12 or earlier satellites. This study examined the previously published cloud detection methods with the intent to develop an automated cloud detection algorithm for NOAA-14 AVHRR data for Texas. Through testing a whole year of AVHRR scenes, the Texas automated cloud detection algorithm was capable of correctly identifying most of the cloud-contaminated pixels except for cloud shadow pixels. The overall accuracy reached 89%. The developed algorithm includes three major steps, top-of-the-atmosphere reflectance of channel 1, temperature difference of channels 3 and 4, and a combination of ratio of channel 2 to channel 1 and temperature in channel 4.

1. Introduction

Cloud contamination appears virtually in almost every Advanced Very High Resolution Radiometer (AVHRR) image. Most research requires cloud-free data, because clouds and cloud shadows influence solar reflectance data and Normalized Difference Vegetation Index (NDVI) values derived from AVHRR data. The NDVI data have been successfully applied to research such as vegetation monitoring (Rasmussen 1998, Duchemin *et al.* 1999), primary production estimation (Ricotta and Avena 1998, Sannier *et al.* 1998) and environmental change detection (França and

e-mail: pyc@nature.berkeley.edu

International Journal of Remote Sensing
ISSN 0143-1161 print/ISSN 1366-5901 online © 2002 Taylor & Francis Ltd
http://www.tandf.co.uk/journals
DOI: 10.1080/01431160110075631

Setzer 1998). Most of the research relied on NDVI data deems to cloud-free by compositing daily images over a ten-day or bi-weekly time period (Holben 1986). A short-period NDVI composite is likely to include cloud-contaminated pixels, which may affect data analysis and may even lead to a false conclusion. Whereas, extended periods of NDVI composites lose the advantage of high temporal resolution of AVHRR data (Gutman 1991), and are not adequate for monitoring agricultural conditions over a short growing season. In addition, Gutman and Ignatov (1996) found that 10-day composites were not cloud-free; moreover, two- or three-week NDVI composites were possibly cloud-contaminated. One of the alternative approaches to overcome cloud-contaminated composites is to detect and remove pixels with cloud obstruction from the daily AVHRR scenes.

Near-real time daily access to AVHRR data over large areas is fundamental to prompt vegetation condition assessment. The major impetus for daily cloud detection is the desire to obtain daily cloud-free AVHRR data and to construct short interval cloud-free NDVI composites for research purposes. Most published cloud detection algorithms are mainly used to study AVHRR data over Europe such as Britain and Germany (Saunders 1986, Dech *et al.* 1998). The state of Texas has very different weather conditions from central Europe. In addition, the state of Texas has experienced drought conditions for the last 10 years. Some cloud detection methods developed in Europe may not be suitable for Texas. Most cloud detection research for AVHRR data has been conducted using data from National Oceanic and Atmospheric Administration (NOAA)-12 or earlier satellites (Saunders 1986, França and Cracknell 1995, Hutchison *et al.* 1997). It is thus important to develop an automated cloud detection method for AVHRR data of Texas received from the NOAA-14 satellite.

2. Objective

Over the years, a number of cloud detection methods has been developed using pixel-by-pixel processing (Saunders and Kriebel 1988, Hutchison and Choe 1996, Cracknell 1997, Hutchison *et al.* 1997, Dech *et al.* 1998). These methods use approaches based on thresholds obtained from all five AVHRR channels as well as systematic mathematical expressions. For general use, most cloud detection schemes for AVHRR data involve the use of surface reflectance (channels 1 and 2) and thermal (channels 3, 4 and 5) data. This involves finding high reflectance pixels in channels 1 and 2 or a ratio close to unity, and low brightness temperature in thermal channels. Cloud detection has been based on the fact that clouds are generally bright in the visible spectrum (channel 1) and/or cold in the infrared spectrum (channel 2) (Gutman 1992), and highly reflective in channel 3 and/or relatively cold in channels 4 and 5 (Yamanouchi and Kawaguchi 1992). Since this study mainly focused on removing cloud-contaminated pixels to improve the accuracy of NDVI values, the cloud detection algorithms were concerned with AVHRR data acquired during the daytime. The objectives of this study were: (1) to apply published methods of cloud detection to AVHRR data over the state of Texas and (2) to develop and test an automated cloud detection algorithm for the state of Texas.

3. Methodology

AVHRR data from NOAA-14 afternoon orbits were downloaded from the High Resolution Picture Transmission (HRPT) receiving station located at Blackland Research and Education Center (part of Texas A&M University complex) in Temple,

Texas. Each AVHRR scene contains five channels. Channels 1 (0.58–0.68 μm) and 2 (0.73–1.1 μm) are solar reflectance channels, and channels 3 (3.5–3.9 μm), 4 (10.3–11.3 μm) and 5 (11.5–12.5 μm) are thermal infrared channels.

Two images (middle and end) of each month between October 1999 and September 2000 were selected for a set of test images to derive radiometric thresholds and to generate a new automated cloud detection algorithm. An additional two images (about 10th and 20th day) for each month during the same period were selected for accuracy assessment of the newly developed cloud detection algorithm. Metadata required for further data pre-processing were retrieved from AVHRR header files by transforming raw data to level 1b format. Automated pixel-by-pixel pre-processing of level 1b data included radiometric calibration for five channels, reflectance conversion for channels 1 (VIS) and 2 (NIR), NDVI computation, satellite zenith, solar zenith and relative azimuth angle computation, and geo-reference correction. Channels 1 and 2 were calibrated and converted to the top-of-the-atmosphere (TOA) reflectance. NDVI values derived from mathematical combination of VIS and NIR were computed for TOA. The three thermal channels were converted from digital counts to brightness temperatures (BT) in degrees kelvin. The three angles were computed in degrees. A geographic information systems (GIS) mask was applied to extract AVHRR data for Texas only.

Cloud contamination in each AVHRR scene can be roughly classified as solid and thick clouds, optically-thin clouds, optical cirrus, cloud edges and cloud shadows (figure 1). The solid and thick clouds consisting of larger particles of ice and/or water are visible as bright-white colour in AVHRR images. The optically-thin clouds in greyish white are usually composed of water particles and/or non-aqueous particles such as smoke and dust. The cirrus clouds are composed of very small ice crystals in the form of grains or ripples (Ahrens 1999). Each AVHRR pixel was visually classified into cloud-contaminated or cloud-free pixels. Cloud-contaminated pixels were then subclassified into thick clouds, thin clouds, optical cirrus, cloud edges and cloud shadows, while cloud-free pixels were subclassified into water, barren lands and vegetation.

3.1. *Threshold test*

For each of 24 study images, four pixels were sampled for each of eight possible cloud-contaminated and cloud-free classes. TOA reflectance in channels 1 (VIS) and 2 (NIR), the computed NDVI, brightness temperature (BT) in channels 3, 4 and 5, and the three angles were recorded for each sample pixel for threshold tests. The tests were based on the published algorithms (Saunders and Kriebel 1988, Hutchison *et al.* 1997). The algorithms included tests of VIS and NIR reflectance individually, ratio of NIR to VIS, BT in channels 4 and 5 individually, and difference between channels 3 and 4, as well as between channels 4 and 5. The published thresholds were set up as 1 for the ratio of NIR to VIS, 233 K for channel 4, and 5 K for the difference between channels 3 and 4. In this study, each of the published thresholds was tested, and unpublished thresholds were justified using Texas data.

3.2. *Accuracy assessment*

In addition to the same pre-processing as the previous 24 test images, another 24 images selected for accuracy assessment were treated with the newly developed algorithm for cloud removal. Pixels that failed any test algorithm were assigned a specific cloud mask value to differentiate them from cloud-free pixels. Raw scenes

served as reference data. Cloud-free scenes were treated as classification data for accuracy assessment. For each of 24 raw scenes, eight pixels were sampled out from each of five cloud-contaminated and three cloud-free classes. A total of 64 pixels was selected from each raw scene. A location of each sampled pixel was recorded by row and column numbers. Each sample from raw scenes was compared to the cloud-free scenes at the same location.

4. Results and discussion

4.1. *Threshold development*

A total of 768 pixels, 480 cloud-contaminated pixels and 288 cloud-free pixels, from 24 sampled images was used for a series of threshold tests. Most cloud detection algorithms using solar reflectance data did not consider bidirectional reflectance distribution function (BRDF). However, Li *et al.* (1996) found that the reflectance was higher in the back scatter direction compared to the forward scatter direction for the same land features, and concluded that this difference was due to the BRDF effect. About half of the Texas data were in the forward scatter direction with a relative azimuth angle close to 180°, while the other half were in the back scatter direction with a relative azimuth angle close to 0°. Reflectance data sampled from different scatter directions were used for developing appropriate thresholds.

4.1.1. *Thresholds of channels 1 and 2*

All of the sampled pixels were used for reflectance comparisons of channels 1 and 2 (figure 2). Our results indicated that cloud-free pixels had lower reflectances between 0 and 0.3 in channels 1 (VIS) and 2 (NIR), whereas cloud-contaminated pixels had higher reflectances and were distributed over large reflectance ranges between 0 and 1.7. Overall, thick and solid clouds had much higher reflectance than other cloud types. The thin cloud and cloud shadow pixels had similar reflectance ranges as cloud-free pixels. Likewise, both cloud shadow and water pixels had a very similar reflectance range; thus, most cloud shadow pixels were confused with water pixels. In addition, some barren pixels were confused with cloud edge pixels. The VIS and NIR reflectances were strongly correlated (R^2 about 0.90) for most cloud-contaminated and cloud-free pixels over barren areas. This indicates that both solar reflectance channels have a similar ability to detect cloudy pixels.

TOA reflectances of cloud-contaminated and cloud-free pixels were plotted (figure 3). Results showed that some land cover types such as barren and vegetation had NIR reflectance data similar to that of most cloudy pixels. Conversely, VIS reflectance data were clearly different between most land pixels and most cloudy pixels. The results were similar to those from previous studies. For example, Saunders and Kriebel (1988) applied NIR reflectance data for cloud detection over sea, and used VIS reflectance data over land features. The reason was that VIS data had lower reflectance over land compared to NIR, which increased the contrast between cloud and land. Since VIS reflectance data could increase the contrast between cloud and land, channel 1 was selected as an appropriate channel from which to develop the automated Texas cloud detection algorithm in this study.

The VIS reflectance data of cloud-free pixels were separated into two groups, back scatter and forward scatter. Most VIS reflectance data over vegetative areas were greater in back scatter direction than in forward scatter direction. For the water and barren pixels, there was no significant difference on the reflectance data between the two scatter directions. A suitable threshold value was required to differentiate

cloud-contaminated from cloud-free pixels for all seasonal data over Texas. The primary goal for finding such a threshold value was to maintain cloud-free pixels as much as possible, while removing cloud-contaminated pixels. The threshold value for Texas data was selected as 0.27 for channel 1 after several iterations and tests. Channel 1 is mainly useful to detect solid and thick clouds, and is applicable for detecting some of optically-thin clouds, optical cirrus and cloud edges over the Texas region.

4.1.2. *Test of brightness temperature difference*

Yamanouchi and Kawaguchi (1992) proposed cloud detection techniques using the brightness temperature (BT) difference between channels 3 (3.7 μm) and 4 (11 μm) during the sunlit season, while applying the difference between channels 4 and 5 (12 μm) irrespective of the season. The difference between channels 3 (T_3) and 4 (T_4) worked well as a cloud discriminator because of high BT at 3.7 μm (T_3) and relatively cold BT at 11 μm (T_4). Hutchison *et al.* (1997) also used difference of T_3 and T_4 for effectively detecting optically-thin cirrus. The difference of T_3–T_4 in figure 4 illustrated that cloud-contaminated pixels had higher temperature differences than cloud-free pixels. Several cirrus and cloud edge pixels were mixed with barren pixels. The cloud shadow pixels had difference values the same as vegetation and water pixels. It was unexpected that some cloud-free water pixels had relatively high temperature differences, while most of the water pixels had values close to 0. The possible explanation is that some water bodies covered by thin clouds or haze cannot be distinguished by human eye. The other possibility is that water pixels are misclassified as thin water clouds due to water vapour above water pixels. In addition, a few barren ground pixels with high temperature differences due to bright surfaces, such as deserts, were confused with clouds. A threshold ΔTc was defined for detecting clouds where T_3–$T_4 > \Delta$Tc. The ΔTc was assigned a value of 11 after several iterations. This criterion is appropriate for detecting thin clouds, most optical cirrus, and cloud edges over Texas.

Other studies by Saunders and Kriebel (1988) and Dech *et al.* (1998) used brightness temperature differences between channel 4 (T_4) and channel 5 (T_5) for detecting thin cirrus and edges of thicker clouds. Differences between T_4 and T_5 were the only cloud detection technique applicable to both daytime and night-time AVHRR data (França and Cracknell 1995). In contrast, results (figure 4) showed that the differences between T_4–T_5 did not differentiate cloud-contaminated from cloud-free pixels over Texas. Results (figure 4) showed that most thick cloud pixels had negative temperature differences, and both cloud-contaminated and cloud-free pixels had overlaps of T_4–T_5 between 0 and 10. In the current study, the algorithm of T_4–T_5 was not adopted as one of the cloud detection steps for Texas.

4.1.3. *Thresholds of channels 4 and 5*

Brightness temperatures in channel 4 (T_4) and channel 5 (T_5) were plotted against each other in figure 5. Linear relationships suggested that T_4 and T_5 were strongly correlated for each class. Most studies used channel 4 for cloud detection algorithms instead of channel 5 because AVHRR data received from NOAA-6 −9 and −12 did not have a spectral information of 11.5–12.5 μm. Hence, channel 5 was not analysed in this study. The general pattern emerged that most cloud-free areas had a higher brightness temperature T_4 than cloud-contaminated areas, because clouds were composed of cold particles such as large ice crystals. In addition, T_4 is sensitive to atmospheric opacity. Both cloud edge and cloud shadow pixels had less or

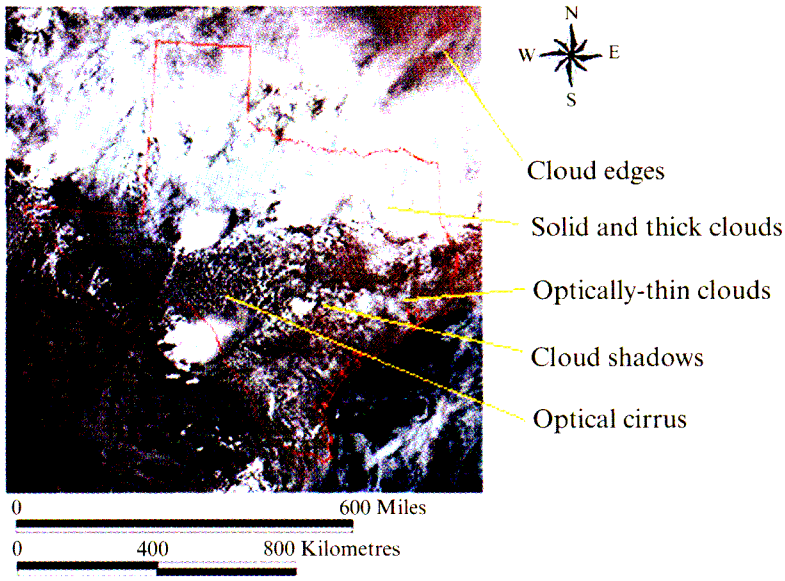

Figure 1. Varieties of cloud contamination scattered on a NOAA-14 AVHRR scene of Texas, USA.

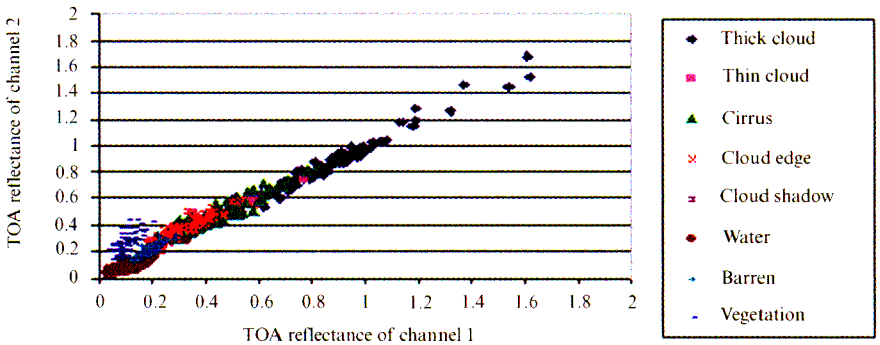

Figure 2. Top-of-the-atmosphere (TOA) reflectance of channel 1 against channel 2.

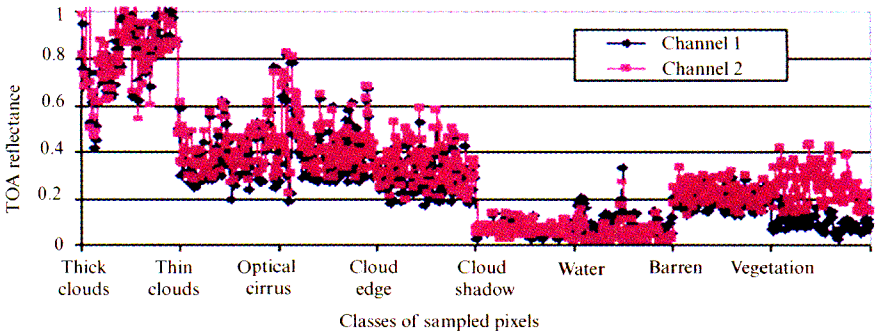

Figure 3. Top-of-the-atmosphere (TOA) reflectance of cloud-contaminated and cloud-free pixels.

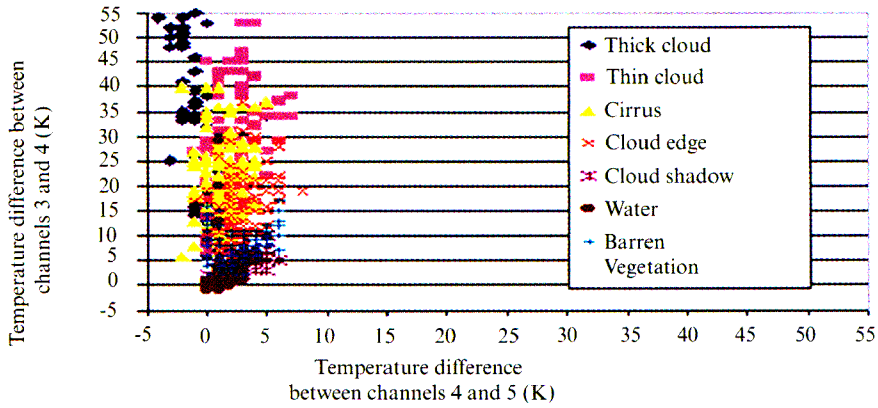

Figure 4. Brightness temperature differences between channels 3 and 4 against difference between channels 4 and 5.

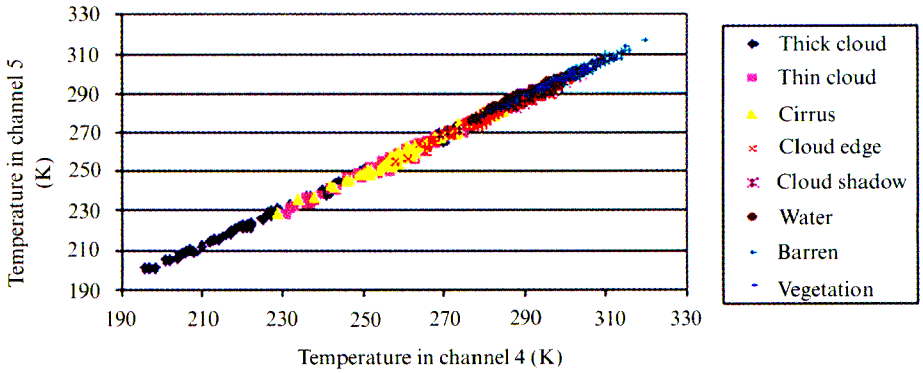

Figure 5. Brightness temperatures in channel 4 against channel 5.

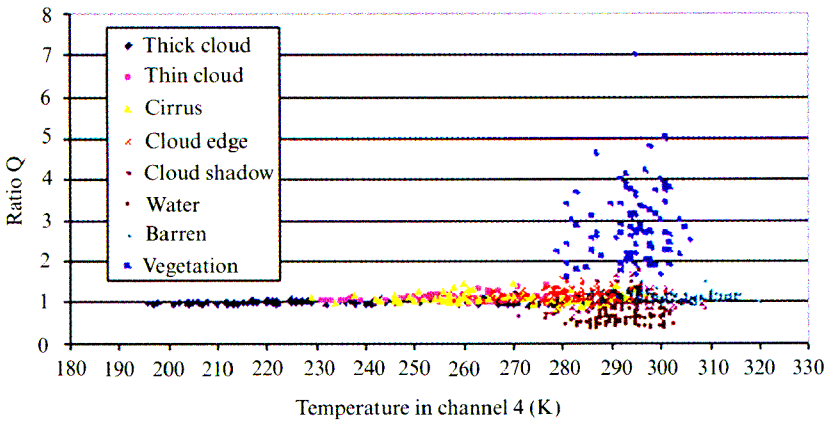

Figure 6. Ratio Q of channel 2 to channel 1 against brightness temperature in channel 4.

no cold particles, and had temperatures similar to cloud-free pixels. Similarly, Yamanouchi and Kawaguchi (1992) concluded that it was very difficult to set a threshold to detect cloudy pixels in channel 4, because many cloud-contaminated and cloud-free pixels had the same BT. Daytime brightness temperature was strongly related to sunlit season and solar radiation. The maximum temperature occurs during July or August, while the coldest temperature occurs in January or February. In addition, the temperature fluctuated with changing weather conditions. Temperatures were usually lower on rainy days and higher during sunny days. Our result suggests that temperature influenced by temporal and weather variables may serve as an important index for manual cloud detection.

Hutchison *et al.* (1997) set the brightness temperature of -40°C (233 K) or colder for channel 4 to detect ice (solid and thick) clouds. This threshold of 233 K was suitable to differentiate thick cloud pixels from other types of cloudy and cloud-free pixels. Since cloudy pixels (except for cloud shadow pixels) can be identified using the VIS reflectance and the difference between T_3 and T_4, the inclusion of a T_4 threshold was expected to improve the differentiation of cloud edge and cloud shadow pixels from cloud-free pixels. The cloud shadow pixels had the same T_4 as water pixels. Moreover, several cloud edge pixels were overlapped with water and vegetative pixels. Overall, the T_4 threshold alone cannot detect all the clouds over Texas.

4.1.4. *Test of ratio of channel 2 to channel 1*

The ratio method of channel 2 reflectance (R_2) to channel 1 reflectance (R_1) was previously applied by Saunders and Kriebel (1988). Several other studies also suggested that this approach was useful. França and Cracknell (1995) concluded that this approach could detect most thin cloudy pixels, and Hutchison *et al.* (1997) applied this approach to detect cirrus clouds. The ratio $Q = R_2/R_1$ was close to unity for most cloudy pixels, less than 0.8 for most cloud-free water pixels, and greater than 1.6 for clear vegetation pixels in Texas (figure 6). França and Cracknell (1995) concluded that the Q values over green vegetation were higher than unity owing to the higher NIR reflectance than VIS reflectance. The VIS reflectance over sea was much greater than NIR reflectance due to the effect of the absorption of water in the near-infrared range. Results indicated that the ratio was appropriate for differentiating cloudy pixels from clear water and vegetative areas over Texas. However, this approach failed to differentiate cloud-contaminated pixels from barren pixels, because the ratio of both pixel types ranged between 0.8 and 1.6. Thus, a supplementary test was added to correctly identify barren pixels from cloud-contaminated pixels. The additional test took account of T_4. The barren pixels had T_4 values greater than 290 K, and could be differentiated from cloud edge and some cloud shadow pixels. Pixels were treated as cloudy if the Q ratio fell between 0.8 and 1.6 and T_4 was less than 290 K. The main purpose of this step is to detect cloud edges and cloud shadows.

4.1.5. *Automated cloud detection algorithm*

The cloud detection algorithm used for Texas included three major steps, TOA reflectance of channel 1, difference of T_3 and T_4, and ratio of R_2 to R_1, associated with T_4. Image pixels that failed in any one of the steps were classified as cloud-contaminated pixels. As a whole, the three major steps of the Texas cloud detection algorithm did not effectively differentiate cloud shadow pixels from barren ground

A couple of visible cloud edge pixels were treated as cloud-free pixels. The possible explanation is that thin or broken cloud edges are smaller than the nominal size of one pixel of 1 km × 1 km. The reason for misidentification of cloud-free water pixels might be caused by the drought situation during the hot summer in Texas. Small lakes in central Texas could be dried out during summertime. Some clear bright surfaces such as barren were mistreated as cloud-contaminated pixels, because both had similar solar reflectance and brightness temperature. More studies are necessary to improve cloud detection algorithms. The complete Texas cloud detection algorithm is presented in figure 7.

5. Conclusion

The Texas automated cloud detection method was applied to individual images. The accuracy of cloud detection was highly related to the threshold values for the three tests. The chosen nominal threshold values were set to accommodate climate conditions between the extreme hot summer and cold winter. The accuracy performance was influenced by image parameters, such as data acquisition time, weather condition, solar zenith angle, satellite scan angle, scatter direction and sunlight.

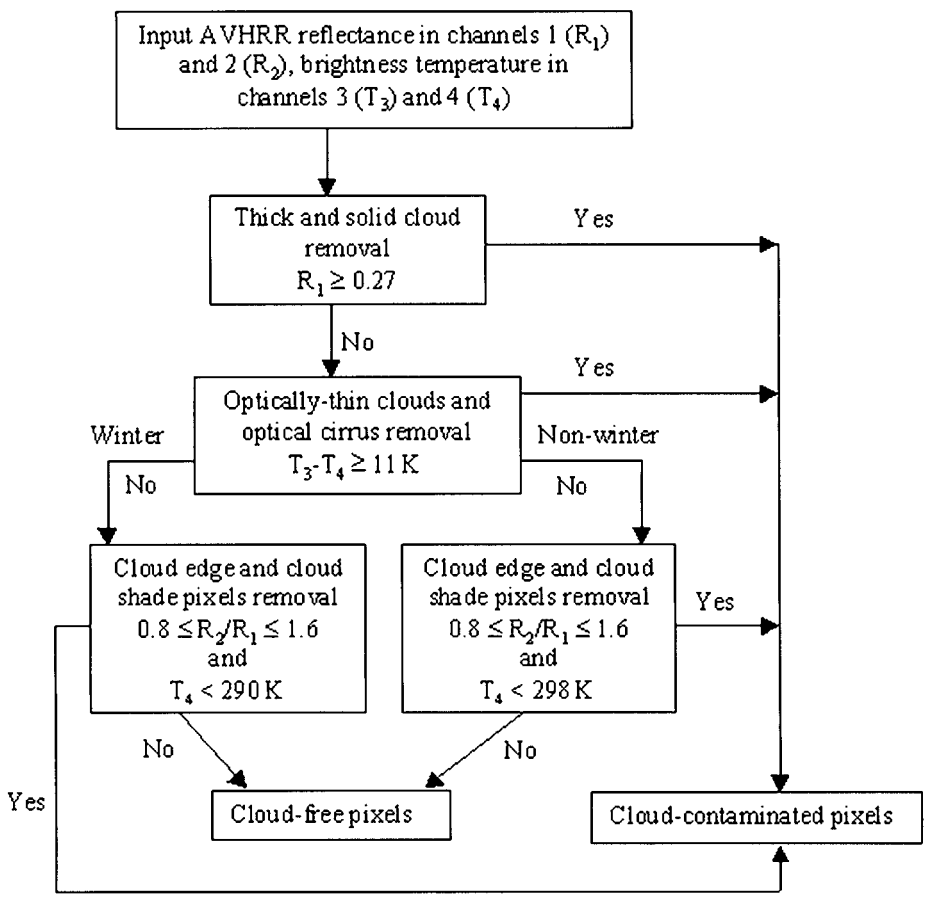

Figure 7. Daytime automated cloud detection algorithm for Texas.

An average of 11% of the cloud-contaminated pixels remained after cloud detection. Maximum value compositing may remove additional cloud-contaminated pixels. A study found that maximum NDVI composites built from cloud-free AVHRR data provided a smooth temporal profile during crop-growing seasons, whereas traditional NDVI composites without the pre-process of cloud detection showed irregular patterns caused mainly by cloud contamination (Chen *et al.* submitted). Cloud removal is important for composite products. The near cloud-free daily AVHRR scenes were appropriate for creating short interval composites for agricultural crop monitoring and other short-term environmental change detection.

Some published cloud detection methods are not functional for Texas data. In addition, thresholds for Texas data are different from those published values. Cloud detection methods and thresholds vary depending on the weather conditions of the study areas. Further research applying the Texas cloud detection algorithm to neighbouring areas with similar weather conditions will be very useful for a regional scale of environmental studies using AVHRR data.

Acknowledgments

The authors would like to thank PCI Geomatics Group in Canada for providing technical assistance in using PCI software, and Dr Robert Baker of the Department of Forest Science at Texas A&M University, USA for providing many helpful comments.

References

AHRENS, C. D., 1999, *Meteorology Today: An Introduction to Weather, Climate and the Environment*, 6th edn (California: Brooks/Cole Publishing).

CRACKNELL, A. P., 1997, *The Advanced Very High Resolution Radiometer* (London: Taylor & Francis).

CHEN, P. Y., SRINIVASAN, R., FEDOSEJEVS, G., and KINIRY, J. R., submitted, Monitoring crop growth in Texas using weekly NDVI composites with/without cloud detection derived from NOAA-14 AVHRR data. *Agronomy Journal*, in review.

DECH, S. W., TUNGALAGSAIKHAN, P., PREUSSER, C., and MEISNER, R. E., 1998, Operational value-adding to AVHRR data over Europe: methods, results, and prospects. *Aerospace Science and Technology*, **5**, 335–346.

DUCHEMIN, B., GUYON, D., and LAGOUARDE, J. P., 1999, Potential and limits of NOAA–AVHRR temporal composite data for phenology and water stress monitoring of temperate forest ecosystems. *International Journal of Remote Sensing*, **20**, 895–917.

FRANÇA, G. B., and CRACKNELL, A. P., 1995, A simple cloud masking approach using NOAA AVHRR daytime data for tropical areas. *International Journal of Remote Sensing*, **16**, 1697–1705.

FRANÇA, H., and SETZER, A. W., 1998, AVHRR temporal analysis of a savanna site in Brazil. *International Journal of Remote Sensing*, **19**, 3127–3140.

GUTMAN, G. G., 1991, Vegetation indices from AVHRR: An updated and future prospects. *Remote Sensing of Environment*, **25**, 121–136.

GUTMAN, G. G., 1992, Satellite daytime image classification for global studies of earth's surface parameters from polar orbits. *International Journal of Remote Sensing*, **13**, 209–234.

GUTMAN, G., and IGNATOV, A., 1996, The relative merit of cloud/clear identification in the NOAA/NASA pathfinder AVHRR land 10-day composites. *International Journal of Remote Sensing*, **17**, 3295–3304.

HOLBEN, B. N., 1986, Characteristics of maximum values composite images from temporal AVHRR data. *International Journal of Remote Sensing*, **7**, 1417–1434.

HUTCHISON, K. D., and CHOE, N., 1996, Application of 1.38 μm imagery for thin cirrus detection in daytime imagery collected over land surfaces. *International Journal of Remote Sensing*, **17**, 3325–3342.

HUTCHISON, K. D., ETHERTON, B. J., and TOPPING, P. C., 1997, Cloud top phase determination from the fusion of signatures in daytime AVHRR imagery and HIRS data. *International Journal of Remote Sensing*, **28**, 3245–3262.

LI, Z., CIHLAR, J., ZHENG, X., MOREAU, L., and LY, H., 1996, The bidirectional effects of AVHRR measurements over boreal regions. *IEEE Transactions on Geoscience and Remote Sensing*, **34**, 1308–1322.

RASMUSSEN, M. S., 1998, Developing simple, operational, consistent NDVI-vegetation models by applying environmental and climatic information. Part II: Crop yield assessment. *International Journal of Remote Sensing*, **19**, 119–139.

RICOTTA, C., and AVENA, G. C., 1998, Fractal modeling of the remotely sensed two-dimensional net primary production pattern with annual cumulative AVHRR NDVI data. *International Journal of Remote Sensing*, **19**, 2413–2418.

SANNIER, C. A. D., TAYLOR, J. C., DUPLESSIS, W., and CAMPBELL, K., 1998, Real time vegetation monitoring with NOAA–AVHRR in Southern Africa for wildlife management and food security assessment. *International Journal of Remote Sensing*, **19**, 621–639.

SAUNDERS, R. W., 1986, An automated scheme for the removal of cloud contamination from AVHRR radiances over western Europe. *International Journal of Remote Sensing*, **7**, 867–886.

SAUNDERS, R. W., and KRIEBEL, K. T., 1988, An improved method for detecting clear sky and cloudy radiances from AVHRR data. *International Journal of Remote Sensing*, **9**, 123–150.

YAMANOUCHI, T., and KAWAGUCHI, S., 1992, Cloud distribution in the Antarctic from AVHRR data and radiation measurements at the surface. *International Journal of Remote Sensing*, **13**, 111–127.